ISSN 0018-151X, High Temperature, 2022, Vol. 60, No. 2, pp. 148–158. © Pleiades Publishing, Ltd., 2022.
Russian Text © The Author(s), 2022, published in Teplofizika Vysokikh Temperatur, 2022, Vol. 60, No. 2, pp. 172–183.

PLASMA INVESTIGATIONS

Distribution of the Rotational Temperature of C_2 Molecules in High-Temperature Regions in a Supersonic Airflow under Injecting Ethylene, Propane, and Oxygen in the Discharge Area

S. I. Inshakov[a, b, *], **V. V. Skvortsov**[a], **V. A. Shakhatov**[c], **E. D. Kudryavtseva**[a], **and A. A. Uspenskii**[a]
[a] *Central Aerohydrodynamic Institute, Zhukovsky, Moscow Oblast, 140181 Russia*
[b] *Moscow Aviation Institute, Moscow, 125080 Russia*
[c] *Topchiev Institute of Petrochemical Synthesis, Russian Academy of Sciences, Moscow, 119071 Russia*
**e-mail: mera@tsagi.ru*

Received October 6, 2020; revised November 8, 2021; accepted November 23, 2021

Abstract—The distribution of the rotational temperature of C_2 molecules in the anode—cathode gap of electric-discharge modules placed in a supersonic flow, observed in the discharge regions under injections of ethylene, propane, and oxygen, are studied with the use of emission spectroscopy. The rotational temperatures of the molecules are assumed to be close to gas-kinetic ones under experimental conditions. The analysis of the alternative way of comparing the gas-kinetic temperature with the rotational temperature of CN molecules shows the latter to be close to a higher vibrational temperature, apparently because CN molecules mainly originate in chemical reactions with the participation of strongly excited components arising under electron impacts. The correlation of the voltage across the discharge gap and the temperatures in the zones of energy release with the dynamic air pressure in the vicinity of the anode is derived.

DOI: 10.1134/S0018151X22010345

INTRODUCTION

Systematic studies of arc and nonequilibrium discharges in supersonic air flows under the injection of additional components into them were started in [1–7]. The techniques for producing mainly longitudinal discharges under simultaneous propane and oxygen injection are described in [8]; they are based on the studies [9–11]. An improved technique for noncontact measurements of the gas-dynamic temperature in high-temperature regions, which arise under these conditions, is presented in [12].

In this study, we describe the results of further spectroscopic studies of the features of origination of these regions with the focus on the possibility of estimating the gas temperature in these regions. Since contact methods are inapplicable to temperature measurements in these regions, the values of the rotational temperature of C_2 molecules, which is the closest to the gas-kinetic temperature, are retrieved from the spectra recorded with the use of the modified method [12], which provides for the values averaged over the rendering line across the heated zone.

INVESTIGATION TECHNIQUE AND RESULTS

The experimental setup has a working part with a rectangular channel 400 mm long with a 120×120 mm^2 cross section. The channel is connected to a profiled rectangular nozzle, designed for a required value of the Mach number M. To produce discharges, electric discharge modules were used (Fig. 1). They consist of a tubular anode mounted downstream and a cathode in the form of a plate with two ledges. The electrodes are made of stainless steel. Anode *3* is hermetically inserted through the wall of flow part *1* using insulator *2* and supplied with fuel and oxidizer. Its shape is convenient for placement in the working part. It ends with the hollow chamber *4*, where a chemically active mixture is produced during discharging and then injected into the flow. Auxiliary fuel is supplied to the chamber through a tube inside the anode. An oxidizer is fed through an outer tube, which is the anode body.

Cathode *6* had the same potential as the metal wall of the working part. The ledge of cathode *5* closest to the anode is intended for a reliable gap breakdown. After igniting the discharge, it was carried by the flow along the cathode and closed mainly to ledge *7*, the farthest from the anode, at a certain value of the discharge current. The anode was fixed either in the center of the working part (Fig. 1a) or near its wall (Fig. 1b). The latter version is designed to use the turbulence effect of the main air—fuel mixture flow near the wall to expand the discharge impact area. The insulator dimensions are chosen so as to exclude sliding breakdown along its surface when a high voltage is applied to the anode.

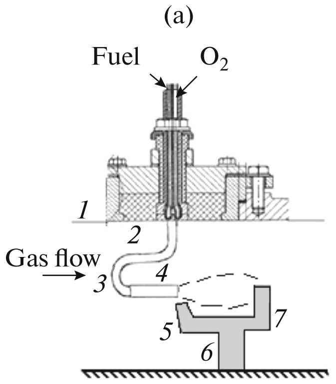

Fig. 1. Schemes of producing a discharge (a) at the center of the working part and (b) near the wall: channel boundary (*1*), insulator (*2*), anode (*3*), hollow chamber at the end of anode (*4*), cathode ledges (*5*, *7*), cathode base (*6*).

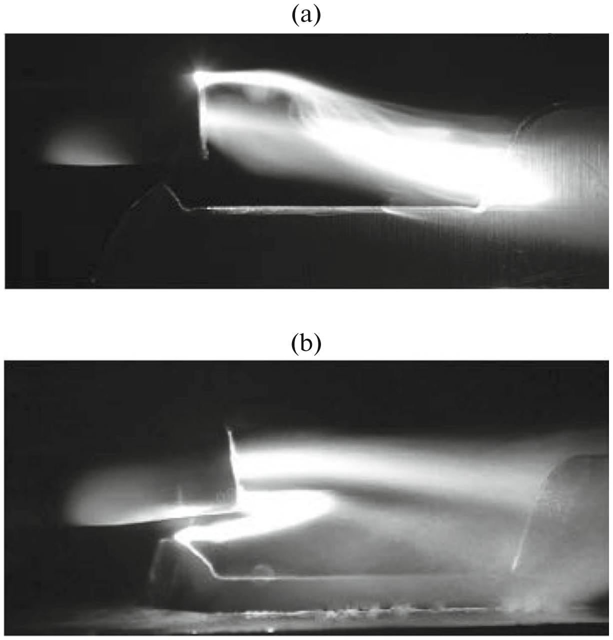

Fig. 2. Pictures of a discharge at voltages across the gap of (a) 1.2 and (b) 0.5 kV.

As can be seen from the geometry of the anodes in Fig. 1, the injection region was far from the place of generation of the head shock wave. Therefore, we can assume that the latter does not affect the flow in the anode–cathode gap. However, this issue, as well as the influence of other spatial gas-dynamic structures on the flow generation in discharge gaps, is beyond the scope of our study.

The experiments were performed at M = 2, a cold flow static temperature of ~160 K, a static pressure of 3.92×10^4 Pa (294 Torr), an injected oxygen excess coefficient of ~2 to 0.95, and discharge currents of 1.5 and 1.8 A. The center of the hole in the anode and the upper edge of the cathode were on the same horizontal line. The space between the ledges of the cathode was 35–37 mm. Figure 2 shows pictures of the discharge made at a discharge current of 1.5 A, injection of ethylene and oxygen at flow rates of 1.5 and 6.15 g/s, respectively, and exposure of 1/500 for the cases where the anode was fixed (a) at the center of the flow and (b) near the unit wall. In case (b), the oxygen flow rate was 7 g/s.

The discharge voltage values turned out to be significantly different in the cases under study: 1.2 kV in case (a) and 0.5 kV in case (b). In the latter case, the discharge closed mainly on the front ledge of the cathode and was close to an arc discharge in terms of the arcing voltage. The discharge voltage decreased to 0.2–0.3 kV as the current increased to 1.8 A. The reason for this difference is explained below.

The main noncontact measuring instrument was a HR4000CG-UV-NIR emission spectrometer with a Toshiba TSD 1304 AP detector; the latter ensured the spectrometer operation in the wavelength range 200–1100 nm (diode array of 3648 elements; inverse dispersion of 0.254 nm/pixel) with an instrument function at the half-maximum of 0.6 nm. Its integration with the experimental setup is described in [8]. The spectrometer received information from the measuring volume ~1 mm diameter in a plane perpendicular to the rendering line and with a length of 5 to 6 mm along that line. The spectrometer was adjusted with the use of a low-pressure DRGS-12 gas-discharge lamp and a graduated SI-8-200 tungsten lamp. The instrument function of the spectrometer was 1.3 nm. The adjacent wavelengths, at which the radiation intensities were recorded, were spaced 0.27 nm apart. Due to the low dispersion of the spectrometer, the methods of unresolved rotational and partly resolved vibrational structures were used to estimate the plasma parameters.

The instrument was used to compare the integral spectra recorded under different conditions for discharging, receiving data on the distribution of radiating components over the interelectrode space, and retrieving the rotational temperature of C_2 molecules.

To record the vibrational-rotational spectra of hydrocarbon components (in this study, C_2 molecules) under the discharge conditions under study, we used the approach generalized in [12], where the particle (atoms, molecules, and their ions) distribution functions over quantum radiating states were retrieved by the multiparameter fitting of the calculated to the experimental emission spectra; the resulting distributions deviated from the Boltzmann distributions in the case of the spectral overlay of the atomic lines and molecular bands in the gas discharge emission. The details of the calculation of the vibrational-rotational spectra of C_2 and the spectra fitting are described in more detail in the Appendix. A distinctive feature of the model used for the calculation of the emission spectra is that it includes a database of measured and calculated spectra and does not require any assumptions about the behavior of the particle distribution functions over excited states. The database was used to test and develop the model. The software codes were adapted to the spectrometer used. Figure 3 shows the distribution of the radiation intensity normalized to the maximum value within the Swan vibrational sequence $\Delta\nu = 0$ of the C_2 molecule in the $d^3\Pi_g \rightarrow a^3\Pi_u$ transition for several values of the rotational temperature T_r calculated with the software.

Similar calculations were also carried out for the sequences $\Delta\nu = -1$ and $\Delta\nu = +1$. It has been ascertained that the short-wavelength part of the spectrum (for example, for the sequence $\Delta\nu = 0$ in the range 490–516 nm) strongly varies with T_r. Hence, the T_r value can be derived from the multiparameter fitting of the calculated to the experimental spectra. This fitting consists of the normalization of the experimental spectrum by subtracting the background value and dividing by the intensity maximum within a sequence and variation in the relative populations of the vibrational levels and the rotational temperature calculated until the spectra matched best.

The comparative analysis of the alternation of the intensities of the bands of the violet system of $CN(B^2\Sigma \rightarrow X^2\Sigma)$ molecule and the Swan system of the $C_2(d^3\Pi_g \rightarrow a^3\Pi_u)$ molecule in the emission spectra of the discharges under study made in [8] and in this study showed the rotational temperatures determined from the levels of the CN molecule to be high, close to the vibrational temperature. This is apparently because the CN molecules originate in chemical reactions with the participation of highly excited components which arise under electron impacts. The rotational temperature values corresponding to the distribution function over the electron-vibrational-rotational levels of the C_2 molecule in the $d^3\Pi_g$ state were closer to the expected values of the gas-kinetic temperature in the gas discharge in a supersonic flow. Therefore, we further used the technique focused on data for these molecules.

For quicker acquisition of information about the rotational temperature, we approximated the parts of the spectra shown in Fig. 3a at wavelengths shorter than 513 nm by exponential distributions (dashed curves in Fig. 3b) with a conditional temperature T_{con}:

$$I = I_{\lambda 0}\exp\left(-\left(hc/kT_{con}\right)\left(1/\lambda - 1/\lambda_0\right)\right),$$

where h is the Planck constant; c is the speed of light; k is the Boltzmann constant; and λ_0 is the wavelength at which a peak near $\lambda = 513$ nm is detected. The relation between T_{con} and T_r turns out to be linear (Fig. 3c). This allows estimating the rotational temperature during the experiment by constructing plots similar to Fig. 3b, deriving T_{con} from them to a specific case, and then retrieving T_r from the linear relation. The rotational temperature found by this technique is exemplified in Fig. 4 (discharge current of 1.5 A, discharge voltage of 1.2 kV, ethylene and oxygen flow rates of 1.5 and 6.15 g/s, respectively).

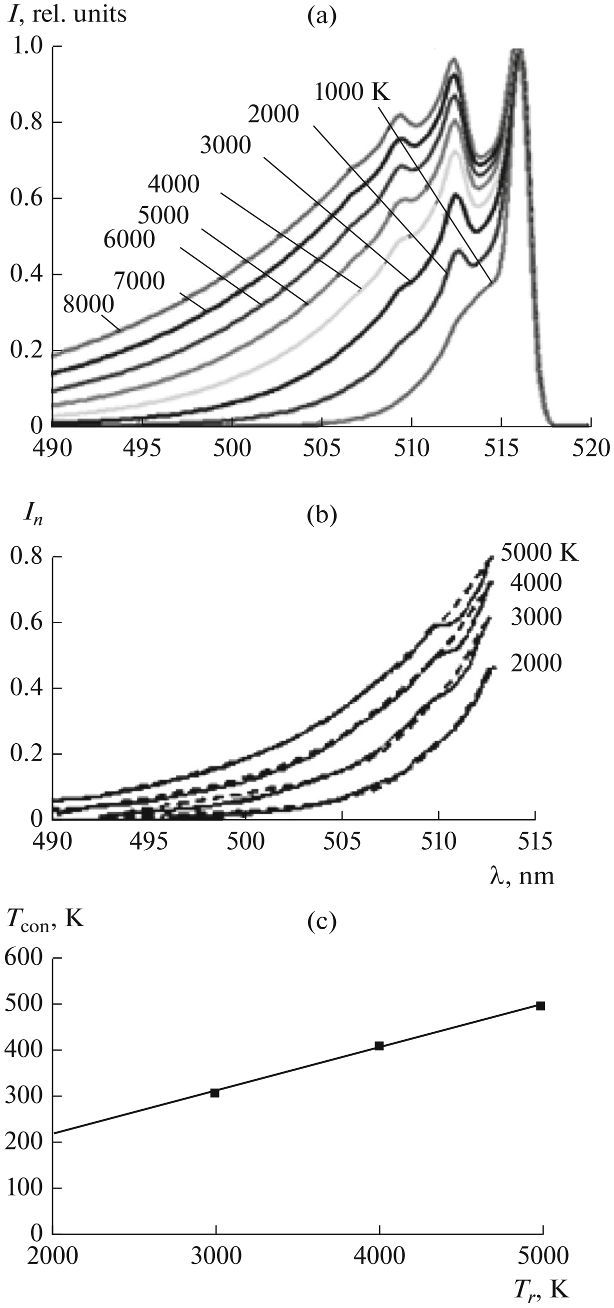

Fig. 3. Calculated dependences of the normalized radiation intensity on the wavelength within the vibrational sequence $\Delta\nu = 0$ of the Swan system of C_2 molecule in the $d^3\Pi_g \rightarrow a^3\Pi_u$ transition for several values of the rotational temperature T_r in the range (a) 490–518 and (b) 490–513 nm; (c) dependence of the conditional temperature on the rotational temperature.

When nonthermal factors do not affect the excitation of molecular levels (for example, under the electron impacts or during the transfer of energy released

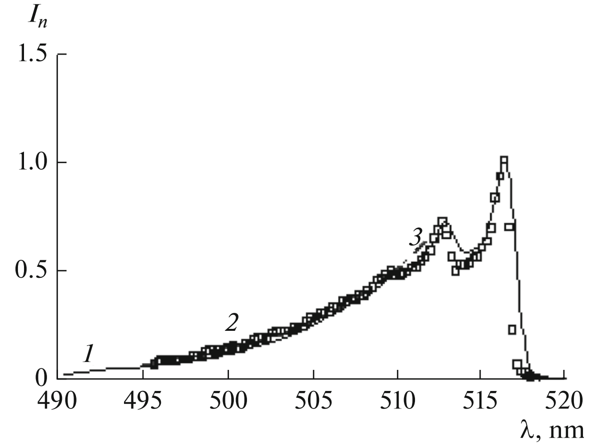

Fig. 4. Example of rotational temperature determined by a simplified method: calculated dependence of the normalized radiation intensity on the wavelength within the vibrational sequence $\Delta v = 0$ of the Swan system of C_2 molecule for a rotational temperature of 4000 K (*1*); distribution experimentally found in the spectrum of ethylene (*2*); exponential approximation for T_r = 4200 K (*3*, dashed curve).

in chemical reactions), the equilibrium between the rotational and translational degrees of freedom of molecules is set after 3–5 intermolecular collisions. In our experiments, the characteristic relaxation time was on the order of 1 μs, which is smaller than the flight time (30–70 μs). Therefore, the gas-kinetic and rotational temperatures were close to each other.

The high speed of data processing by the spectrometer made it possible to receive information on the radiation intensity distribution in the emission spectra in a discharge cross section for one operation cycle of the aerodynamic setup.

The comparison of the integrated spectra recorded at high and low discharge voltages in the regions of the strongest radiation at a discharge current of 1.5 A is shown in Fig. 5.

The distributions of some emitting components in the middle of the discharge gap across the discharge are shown in Fig. 6 (the Y coordinate is measured from the horizontal line which connects the center of the chamber at the end of the anode and the edge of the far ledge of the cathode). These experimental data show the significantly different nature of the processes (in particular, arising of electron temperatures, chemical reactions) responsible for the emission. At a low discharge voltage, the emissions of CN and CH molecules and hydrogen atoms was weakly distinguished from the C_2 emission, in contrast to the discharge at a high voltage between the electrodes.

The decrease in the discharge voltage results in a decrease in the energy input and the gas-kinetic temperature. This is also shown in the rotational temperatures of C_2 molecules. The height distribution of this temperature at the center of the discharge gap (X = 16.5 mm from the chamber section at the end of the anode) at a discharge current of 1.5 A is shown in Fig. 7 for high (*1*) and low (*2*) discharge voltages.

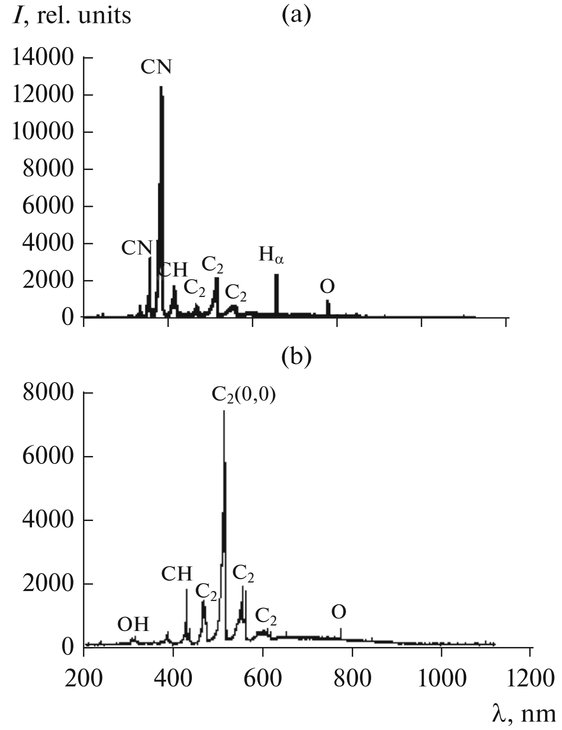

Fig. 5. Comparison of the integral spectra of a discharge at high and low voltages: (a) U = 1.2 kV, ethylene flow rate is 1.5 g/s and oxygen flow rate is 6.15 g/s; (b) U = 0.3 kV, ethylene flow rate is 1.27 g/s and oxygen flow rate is 8.4 g/s.

When producing discharges following the scheme shown in Fig. 1b, it is desirable that the discharge occupies the whole interelectrode gap between the cathode ledges. Taking into account the previous experience of working with similar discharges [8–11], we assumed the cause of the discharge closure mainly to the front ledge of the cathode in the experiments—the low dynamic air pressure in the gap between the horizontal section of the anode and the plate where the cathode was mounted due to deceleration of the airflow over this gap. To verify this assumption, the length of the horizontal section of the anode was decreased to the minimum acceptable in the anode manufacturing technology (in our case, from 85 to 42 mm). This change actually led to the discharge development over a much longer distance and an increase in the discharge voltage to 1–1.4 kV. The corresponding studies have been performed with ethylene and propane as auxiliary gases. The height distributions of the rotational temperature over the discharge gap for these gases at a discharge current of 1.5 A are shown in Fig. 8 for a number of distances from the anode section.

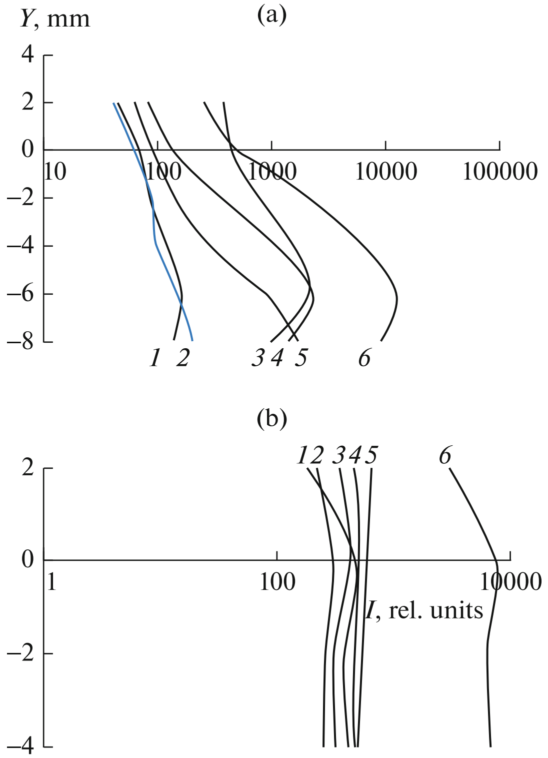

Fig. 6. Distributions of the relative emission intensity of (a) CH (*1*), OH (*2*), C_2 (*3*), H_α(*4*), O (*5*), and CN (*6*); (b) CH (*1*), OH (*2*), CN (*3*), H_α (*4*), O (*5*), and C_2 (*6*), derived from processing the integral spectra, over the middle section of the discharge gap at high (a) and low (b) discharge voltages.

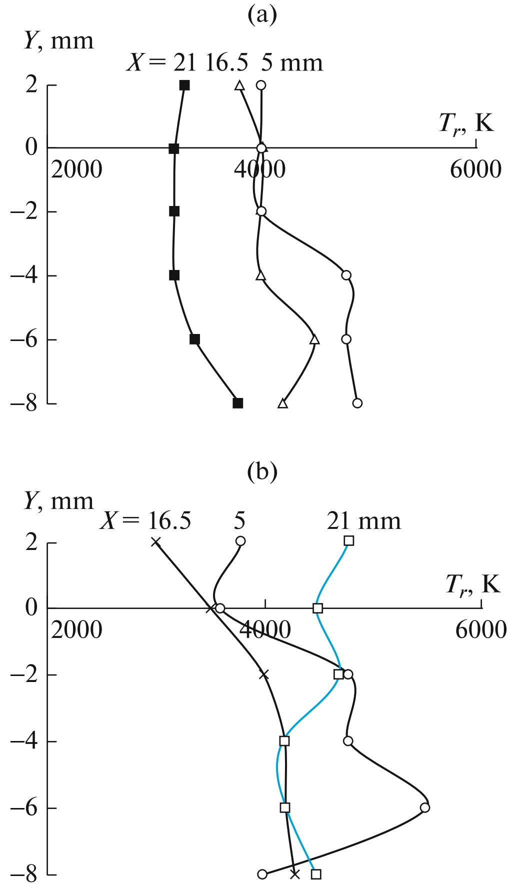

Fig. 8. Height distributions of the rotational temperature over the discharge gap derived at different distances from the anode cross section for (a) ethylene and (b) propane at a discharge current of 1.5 A and an anode horizontal section length of 42 mm.

The coordinate system is the same as in Fig. 6. In the experiments with ethylene, its flow rate was 1.5 g/s and the oxygen flow rate was 6.2 g/s (oxygen excess coefficient $\alpha \approx 1.2$); and the discharge voltage was 0.95–1 kV. When propane was used, its flow rate also was 1.5 g/s and the oxygen flow rate was 7.14 g/s ($\alpha \approx 1.3$); and the discharge voltage was 1.1–1.2 kV. The results show a shift of the main heat release zone below the coordinate $Y = 0$ in both cases, as well as the inhomogeneity of the energy release in the studied zone.

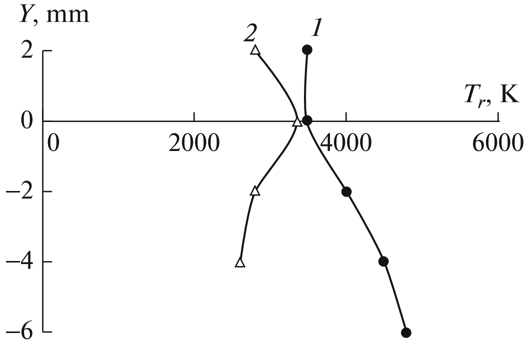

Fig. 7. Height distribution of the rotational temperature of C_2 molecules over the discharge gap at high and low discharge voltages: $U = 1.2$ kV, ethylene flow rate is 1.5 g/s and oxygen flow rate is 6.15 g/s (*1*); $U = 0.3$ kV, ethylene flow rate is 1.27 g/s and oxygen flow rate is 8.4 g/s (*2*).

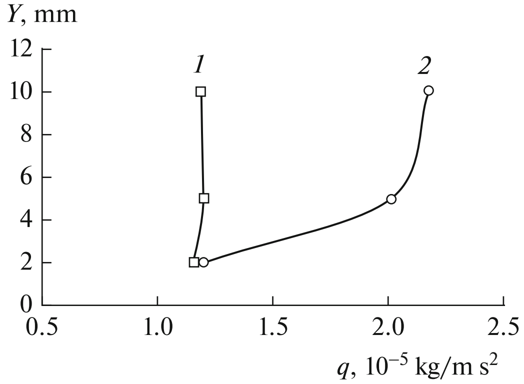

Fig. 9. Dynamic air pressure distribution over the gap between the lower anode edge and the plate at horizontal anode section 85 (*1*) and 42 mm long (*2*).

When using propane, higher maximum temperatures were recorded than for ethylene; i.e., the same situation took place as in the corresponding flames. At the same distance from the anode, $X = 21.5$ mm, the temperature in the case of propane turned out to be higher than in the case of ethylene. In the experiments performed, temperatures of 3500 to 4500 K were attainable, which was higher than in the ethylene-oxygen and propane-oxygen flames (~3000 K) or in the supersonic air flow heated by a nonequilibrium discharge at a comparable electric power supply and equal static pressure (~2000 K).

To verify the assumption about the role of the dynamic air pressure in formation of the region with a high temperature behind the anode in the absence of a discharge, the static and total pressures were measured with pneumometric sensors in the gap between the lower edge of the anode and the plate at the anode with horizontal sections of 42 and 85 mm in length. These data were used to calculate the values $q = \rho w^2$ [kg/m s^2], where ρ is the gas density and w is its speed in the flow. The measurements performed in the section of the anode output channel between its lower horizontal edge and the plate are shown in Fig. 9. According to them, the dynamic air pressure near the anode is approximately half the pressure in the case of a long horizontal section than in the case of a short horizontal section of the anode.

The significant effect of the discharge current on the rotational temperature of the C_2 molecules ascertained in the experiment with an anode with a shorter horizontal section and a combination of propane with oxygen as injected gases (1.5 and 7.14 g/s, respectively) is shown in Fig. 10.

CONCLUSIONS

The emission spectroscopy study of the temperature and its distribution in zones formed in high-speed air flows by longitudinal and near-longitudinal DC discharges under the injection of hydrocarbon fuels and oxygen into them has shown the origination of high-temperature zones with temperatures higher than in the usual ethylene-oxygen and propane-oxygen flames or in a supersonic air flow heated by a nonequilibrium discharge at comparable values of the electric power supply and equal static pressures. The results indicate that an increase in the dynamic air pressure in the main flow leads to the transformation of the discharge zone where plasma-chemical reactions take place, its elongation, and an increase in the discharge voltage and temperature.

APPENDIX

The multiparameter fitting (see below) is based on the analysis [12] of the calculations of electron-rotational-vibrational (ERV) C_2 spectra.

High-intensity ERV molecular bands which corresponded to the Swan $C_2(d^3\Pi_g \to a^3\Pi_u)$ system are considered in the analysis, taking into account the fact that the electric dipole transition between the triplet electronic states $d^3\Pi_g$ and $a^3\Pi_u$ of the C_2 molecule is determined by the selection rules, the bond type (interactions between electrons and particle nuclei), and the symmetry properties of these states [13, 14].

The power per unit volume $\varepsilon_{mn}(\tilde{\nu}_{\text{rad}} - \tilde{\nu}_{mn})$ emitted by the C_2 molecules during the electric dipole transition $m \to n$ (m and n mean sets of quantum numbers) per unit wavenumber range was calculated within the quantum electrodynamics and physical kinetics [13–18]. The position of the C_2 ERV line in the emission spectrum, which corresponds to the $m \to n$ transition, is determined by the wavenumber $\tilde{\nu}_{mn}$. It was assumed that the wavelengths of the electromagnetic field are much larger than the size of the C_2 molecule. This condition is valid in the ultraviolet, visible, and infrared wavelength regions, which are of interest for practical spectroscopy. The electromagnetic field interacting with the C_2 molecule is weak. This interaction results in the absorption and emission of one photon. The photon energy is equal to the energy difference between the quantum states of the C_2 molecule, which are specified by the selection rules for the electric dipole transition of the C_2 molecule. The emission spectra of the C_2 molecule in the high-temperature zone between the electrodes are mainly due to the spontaneous emission of the C_2 molecule in the $d^3\Pi_g$ excited state. The dependence of $\varepsilon_{mn}(\tilde{\nu}_{\text{rad}} - \tilde{\nu}_{mn})$ on the particle concentration N_m in the excited radiating state $d^3\Pi_g$ is defined by the expressions [13–18]:

$$\begin{gathered}\varepsilon_{mn}(\tilde{\nu}_{\text{rad}} - \tilde{\nu}_{mn}) = S_{mn}(\tilde{\nu}_{\text{rad}} - \tilde{\nu}_{mn})\,\varepsilon_{mn}^{\text{int}}(\tilde{\nu}_{mn}), \\ \varepsilon_{mn}^{\text{int}}(\tilde{\nu}_{mn}) = A_{mn}N_m hc\tilde{\nu}_{mn}.\end{gathered} \tag{1}$$

Here, $\varepsilon_{mn}^{\text{int}}(\tilde{\nu}_{mn})$ is the power emitted by C_2 molecules per unit volume and A_{mn} is the spontaneous

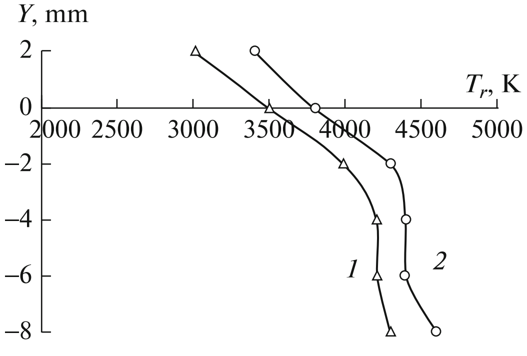

Fig. 10. Height distribution of the rotational temperature over the discharge gap in the middle zone at a discharge current of 1.5 (*1*) and 1.8 A (*2*).

emission probability. The function $S_{mn}(\tilde{\nu}_{\rm rad} - \tilde{\nu}_{mn})$ of the wavenumber $\tilde{\nu}_{\rm rad}$ shows the real profile of the ERV line, which corresponds to the electric dipole transition of the C_2 molecule.

In the model for emission spectra calculation, the inhomogeneous Doppler and homogeneous ERV line broadening [19] caused by the thermal motion of C_2 molecules and the interaction between heavy particles (molecules and atoms), respectively, were considered. When homogeneous broadening is taken into account in the model, the line broadening due to collisions between heavy particles is assumed to be much more significant than the natural broadening, and the line shift due to particle collisions at the gas-kinetic temperature $T_g \geq 2000$ K is much smaller than its Doppler broadening. The homogeneous broadening of ERV lines in the spectrum of the C_2 molecule was estimated with the use of models of hard spheres (with different approximations of the dependence of the particle collisional cross section on the temperature T_g) and models where the interaction potential in particle collisions is approximated by the Lennard–Jones or Born–Meier potential [20]. Accounting for the homogeneous and inhomogeneous line broadening determined the dependence of the $\varepsilon_{mn}(\tilde{\nu}_{\rm rad} - \tilde{\nu}_{mn})$ value on the interaction potential parameters and the translational gas temperature T_g in the high-temperature zone.

The use of the adiabatic approximation [13–18] for the diatomic molecule C_2 admits the series of transformations of Eq. (1):

$$\varepsilon_{mn}^{\rm int}(\tilde{\nu}_{J'J''}) = \frac{16\pi^3 c}{3}\tilde{\nu}^4_{J'J''} S_{e'_{st}e''_{st}}(r_{v'v''}) q_{v'v''} \times \frac{S_{J'J''}}{(2J'+1)K'} N_{J'v'e'_{st}}.$$

Here, m and n are expressed in terms of the quantum numbers v', J' and v'', J'', respectively. The superscript "'" designates the upper radiating state $e'_{st} = d^3\Pi_g$ of the C_2 molecule, and the superscript ″, the lower electronic state $e''_{st} = a^3\Pi_u$; J' and J'' are the quantum numbers of the total angular momentum of molecular rotation; $\tilde{\nu}_{J'J''}$ is the wavenumber which determines the position of the ERV line in the molecular spectrum; $S_{J'J''}$ is the strength of the ERV line (Hönl–London factor); $S_{e'_{st}e''_{st}}(r_{v'v''})$ is the strength of the $J', v', e'_{st} \to J'', v'', e''_{st}$ electronic transition; $N_{J'v'e'_{st}}$ is the concentration of C_2 molecules in the excited ERV state $J', v', e'_{st} = d^3\Pi_g$; K' is the normalizing coefficient of the Hönl–London factor [18]; $r_{v'v''}$ is the r-centroid; and $q_{v'v''}$ is the Franck–Condon factor. The values of $S_{J'J''}$ and the sets of quantum numbers J', v', e'_{st} and J'', v'', e''_{st} are determined by the intermediate coupling by Hund ([13], pp. 426–430), symmetry properties of the upper and lower ERV states of the C_2 molecule, and selection rules for electric dipole transitions $J', v', e'_{st} \to J'', v'', e''_{st}$ [13–15].

The databases have been created for the calculation of the $\varepsilon_{mn}^{\rm int}(\tilde{\nu}_{mn})$ value based on a number of works (for example, [13, 18, 21–26]); they include the spectroscopic constants of electronically excited states of the C_2 molecule; and values of $S_{e'_{st}e''_{st}}(r_{v'v''})$, $q_{v'v''}$, wavelengths, and the probability of radiative transitions of the C_2 molecule. The $S_{e'_{st}e''_{st}}(r_{v'v''})$ values are calculated by the semiempirical expression [18]:

$$S_{e'_{st}e''_{st}}(r_{v'v''}) = 33(1 - 0.52 r_{v'v''})^2.$$

The positions of rotational lines $\tilde{\nu}_{J'J''}$ in the spectrum are determined with allowance for the intermediate type of coupling by Hund, the selection rules, and the symmetry properties of the ERV states by the relationship [13–15, 18]:

$$\tilde{\nu}_{J'J''} = \tilde{\nu}_{v'v''} + F(J', v') - F(J'', v'').$$

To calculate the spectral rotational terms $F(J', v')$ and $F(J'', v'')$ in the vibrational states v' and v'', respectively, the expressions from [13–18] are used, which take into account rotational-vibrational, centrifugal, and spin-orbital interactions. The ensemble of the ERV lines observed in the C_2 molecule emission spectrum is caused by the transitions between different rotational levels J' and J'' at fixed values of the vibrational states v' and v''. The value of $\tilde{\nu}_{v'v''}$ is constant in the calculation of $\tilde{\nu}_{J'J''}$ for the specific electronic-vibrational transition $\nu', e'_{st} = d^3\Pi_g \to \nu'', e''_{st} = a^3\Pi_u$ [14, 15]. It determines the beginning of the electronic-vibrational band (zero line) and is calculated in the model by the expression [13–18]:

$$\tilde{\nu}_{v'v''} = \tilde{\nu}_{e'_{st}e''_{st}} + G(v') - G(v'').$$

The value of $\tilde{\nu}_{e'_{st}e''_{st}}$ is defined as the difference between the values of the upper $T_{e'_{st}}$ and lower $T_{e''_{st}}$ states of the spectral electronic terms which correspond to the $e'_{st} = d^3\Pi_g$ and $e''_{st} = a^3\Pi_u$ states:

$$\tilde{\nu}_{e'_{st}e''_{st}} = T_{e'_{st}} - T_{e''_{st}}.$$

This difference is constant during the electronic-vibrational transition $\nu', e'_{st} = d^3\Pi_g \to \nu'', e''_{st} = a^3\Pi_u$.

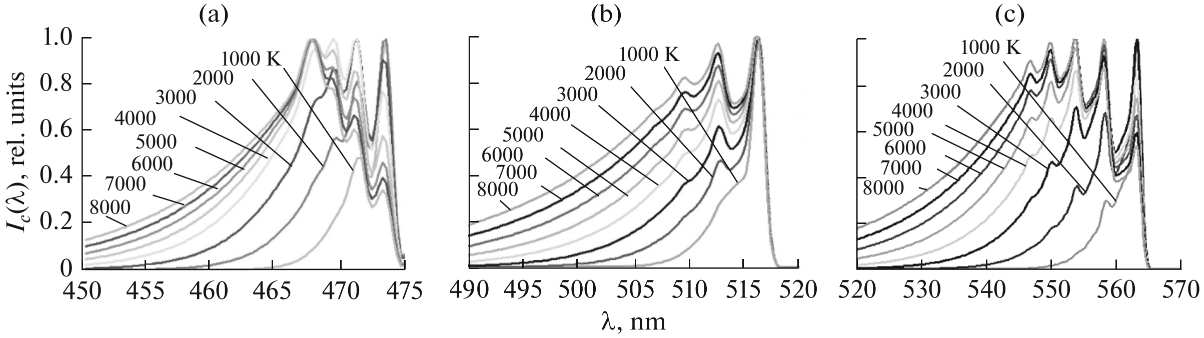

Fig. 11. Intensity $I_c(\lambda)$ distribution in the Swan sequence bands of the C_2 molecule in the translational temperature range T_g = 1000–8000 K at equilibrium between the translational and internal degrees of freedom of the molecule: (a) $\Delta v = -1$, (b) $\Delta v = 0$, (c) $\Delta v = +1$.

The values of $G(v')$ and $G(v'')$ are determined by the spectral vibrational terms which correspond to the upper $e'_{st} = d^3\Pi_g$ and lower $e''_{st} = a^3\Pi_u$ electronic states of the C_2 molecule. The values of $G(v)$ are calculated in the model based on the relation from the works [13–18].

The intensity distribution in certain regions of the ERV emission spectrum of molecules during electric discharges can be characterized by different values of the rotational temperature ("cold" and "hot" regions of the molecular emission spectra) [13]. The appearance of cold and hot sections in the spectra is due to the physicochemical processes with the participation of molecules in electronically excited states. In contrast to the models for calculating emission spectra ([27–29] and others), the computational codes we have created in this study allow us to determine the set of $T_{\mathrm{rot}}(e'_{st})$ values corresponding to different rotational terms and selected groups of quantum numbers.

Multiparameter Fitting of the Calculated to the Experimental Spectra

Before the fitting procedure, the calculated and experimental spectra are converted into one format convenient for the comparison. Alternation of the intensity $I_c(\lambda)$ versus the wavelength λ in the spectra is normalized to the intensity maximum.

The procedure of multiparameter fitting of the calculated to measured spectra consists of the following steps.

To speed up the processing of the experimental data, a data set is created: during the first stage of the fitting, a library of intensity dependences $I_c(\lambda)$ is calculated for the bands belonging to sequences ($\Delta v = 0, \pm 1$) of the Swan system ($d^3\Pi_g \rightarrow a^3\Pi_u$) of the C_2 molecule at the rotational temperatures $T_r(d^3\Pi_g)$ = 1000–8000 K. During this stage, the rotational temperature $T_r(d^3\Pi_g)$ is assumed to be equal to T_g and the vibrational temperature $T_V(d^3\Pi_g)$, which corresponds to the Boltzmann distribution function of C_2 molecules over the electronic-vibrational levels v' of the state $e'_{st} = d^3\Pi_g$. The $T_{\mathrm{r}}(d^3\Pi_g)$ maxima and minima are determined from the comparison with the experimental spectra, at which

$$I_c^{\min}(\lambda) \le I_{\exp}(\lambda) \le I_c^{\max}(\lambda). \quad (2)$$

Here, $I_c^{\min}(\lambda)$ and $I_c^{\max}(\lambda)$ are the intensities calculated under the condition of minimal differences $I_{\exp}(\lambda) - I_c^{\min}(\lambda)$ and $I_c^{\max}(\lambda) - I_{\exp}(\lambda)$. Figure 11 shows the calculated intensity distributions as functions of the wavelength in the band sequence ($\Delta v = 0, \pm 1$) of the Swan system of the C_2 molecule at different values of $T_r(d^3\Pi_g)$ and equilibrium between the translational and internal degrees of freedom of the molecule. According to the calculations, the spectral region which corresponds to short wavelengths strongly changes with $T_r(d^3\Pi_g)$.

During the second stage of fitting, five $N_{e'_{st}v'} / N_{e'_{st}v'=0}$ values (v' = 1–5) found during the first stage at the temperature $T_r(d^3\Pi_g)$ are changed to satisfy condition (2); $T_g = T_r(d^3\Pi_g)$.

During the third stage, the $T_r(d^3\Pi_g)$ value is changed at the $N_{e'_{st}v'} / N_{e'_{st}v'=0}$ values found during the second stage to satisfy condition (2). As in the previous stages, $T_g = T_r(d^3\Pi_g)$.

The next stages of the fitting repeat the second and third stages until the best agreement between the measured and calculated intensity dependences $I_c(\lambda)$ in the bands of different sequences ($\Delta v = 0, \pm 1$) of the Swan system of the C_2 molecule. If the $T_r(d^3\Pi_g)$ values, which correspond to the bands from different sequences, coincide, then we analyze the conditions under which the $T_r(d^3\Pi_g)$ value found can be identi-

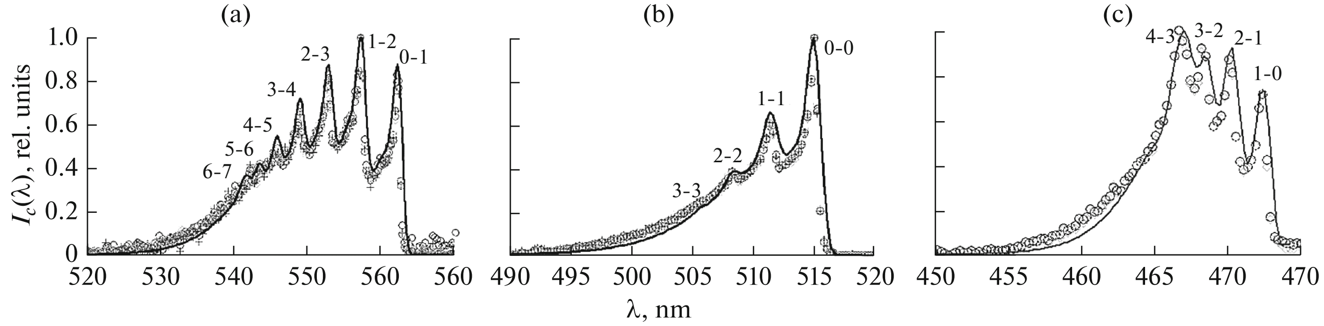

Fig. 12. Distributions of the measured (symbols) and calculated (solid lines) intensity $I_c(\lambda)$ in the bands of the Swan C_2 sequence under imbalance between the rotational and vibrational degrees of freedom of the molecule in the $d^3\Pi_g$ state: (a) $\Delta v = -1$, T_r $(d^3\Pi_g) = 2230 \pm 300$ K, and $T_V(d^3\Pi_g) = 5800 \pm 900$ K for v = 0–2; (b) $\Delta v = 0$, 2300 ± 300 K, and 6600 ± 900 K; (c) $\Delta v = +1$, 2000 ± 300 K, and 6000 ± 900 K.

fied with the gas-kinetic temperature T_g in the high-temperature zone. They correspond to [13].

The relaxation time of the energy τ_{R-T} stored in the ERV degrees of freedom of the C_2 molecule should be longer than the translational relaxation time $\tau_{T-T}$of the molecule and shorter than the spontaneous radiative decay time $\tau_{e'_{st}}$, which corresponds to the $d^3\Pi_g \to a^3\Pi_u$ transition of the C_2 molecule: $\tau_{T-T} < \tau_{R-T} \ll \tau_{e'_{st}}$. To estimate τ_{R-T}, the characteristic time is assumed to be comparable with the translational relaxation time of the C_2 molecule in order of magnitude. The τ_{T-T} value is on the order of magnitude of the average time of collisions of C_2 molecules with particles in the high-temperature zone, $\tau_{T-T} \approx (2–5) \times 10^{-9}$ s in the temperature range from 1000 to 5000 K; and $\tau_{e'_{st}} = (1–8) \times 10^{-7}$ s [18]. The condition $\tau_{R-T} \ll \tau_{e'_{st}}$ is satisfied in the high temperature zone.

The characteristic times of direct and reverse inelastic processes and chemical reactions with the participation of C_2 molecules in the excited $d^3\Pi_g$ state are assumed to be much longer than the times τ_{R-T} and $\tau_{e'_{st}}$.

The residence time of C_2 molecules in the excited $d^3\Pi_g$ state in the high-temperature zone should be longer than the times τ_{R-T} and $\tau_{e'_{st}}$. This condition is satisfied since $\tau_L \approx (3–7) \times 10^{-5}$ s [30]. As is ascertained in this study, T_r $(d^3\Pi_g)$ increases with the energy input in the discharge zone. This also indirectly points to the fact that T_r $(d^3\Pi_g) = T_g$. Thus, the gas-kinetic temperature T_g coincides with the rotational temperature $T_r\left(d^3\Pi_g\right)$ in the high-temperature zone.

The results of calculation of the rotational temperature $T_r(d^3\Pi_g)$ via multiparameter fitting are shown in Fig. 12. The symbols correspond to the intensities measured under the conditions of an electric longitudinal discharge discussed in detail in [8–10]. The solid curves show the intensity calculated. The distribution function over the ERV levels of the C_2 molecule in the $d^3\Pi_g$ triplet state is satisfactorily described by the Boltzmann distribution; the rotational temperatures corresponding to different sequences coincide within the error (±300 K) and lie in the T_r $(d^3\Pi_g)$ 2000–2300 K range. Propane C_3H_8 with the mass flow rate $G_{C_3H_8} = 1$ g/s is introduced into the interelectrode region. The emission spectra were recorded in a cross section of the discharge channel located at the distance $X = 21$ mm from the leading edge of the cathode [8–10].

The model used for the calculation of the emission spectra is distinctive in that it does not require any assumptions about the behavior of the distribution functions of C_2 molecules over the vibrational levels v'. The comparison between the measured and calculated emission spectra in the high-temperature zone allows deriving the $N_{e'_{st}v}/N_{e'_{st}v'=0}$ values from the dependence

$$\ln(N_{e'_{st}v'}/N_{e'_{st}v'=0}) = f\left(hcG\left(v'\right)\right),$$

which is the desired distribution function of C_2 molecules over the electronic-vibrational levels in the state $e'_{st} = d^3\Pi_g$. In the case of its linear dependence on $hcG\left(v'\right)$, the distribution function of C_2 molecules over electronic-vibrational levels v' is Boltzmann. The concept of the vibrational excitation temperature T_v $(d^3\Pi_g)$ for the given vibrational levels v' of the state $e'_{st} = d^3\Pi_g$ is introduced into the model. Its value is determined by the slope of the straight line constructed by the least squares method for the dependence of $\ln(N_{e'_{st}v'}/N_{e'_{st}v'=0})$ on $hcG\left(v'\right)$. Figure 13 shows the distribution function over the electronic-vibrational levels v' of the C_2 molecule in the $d^3\Pi_g$ excited state.

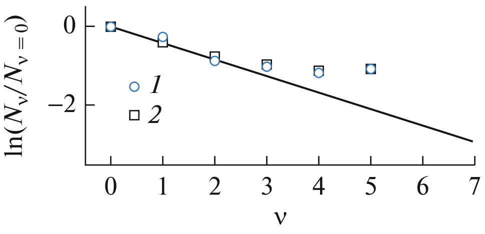

Fig. 13. Distribution function over vibrational levels v of the C_2 molecule in the $d^3\Pi_g$ excited state (symbols) derived from processing of the emission spectra of the Swan sequences $\Delta v = 1$ (*1*) and 0 (*2*): calculation by the Boltzmann formula at the vibrational temperature T_v ($d^3\Pi_g$) = 6000 K (line); N_v is the concentration of C_2 molecules excited to the vibrational level v; the conditions are the same as in Fig. 12.

It has been ascertained that the state of an ionized gaseous medium in the interelectrode zone is nonequilibrium [8–10]. For all sequences, the distribution function over six electronic vibrational levels (v' = 0–5) is not described by the Boltzmann distribution. The distribution function over three electronic vibrational levels (v' = 0–2) is Boltzmann with the temperature 5800–6600 K, which exceeds the rotational temperature (2000–2300 K). The temperature hierarchy corresponding to different degrees of freedom of the C_2 molecule has the form

$$T_v(d^3\Pi_g) > T_r(d^3\Pi_g) \approx T_g.$$

The database of the measured and calculated spectra is used to validate and develop the model. Figure 14 shows the emission spectra of the C_2 molecule calculated within the model developed in this study and with models [27–29]. A satisfactory agreement is observed between the calculation results and rotational and vibrational temperatures determined with the use of different models.

Processing the emission spectra consists of identification of the spectrum, background subtraction, and determination of the spectral response and the transfer function of the optical system. It is assumed that the intensity of the observed emission spectra of C_2 molecules in the high-temperature zone is not distorted due to reabsorption, refraction, rereflection from elements of the optical system, etc.

During identification of the spectra from the high-temperature zone, tabular data [21] and the spectra comparison method [13] are used. The identified spectra from different published sources [13, 22–32] are used in the spectra comparison method. To determine the background intensity, spectral regions free of atomic lines and molecular bands are considered. The calibration characteristics of the optical system make it possible to take into account the distortion of the spectral intensity distribution due to the interaction of the electromagnetic radiation with the elements of the working part of the experimental setup and the optical system.

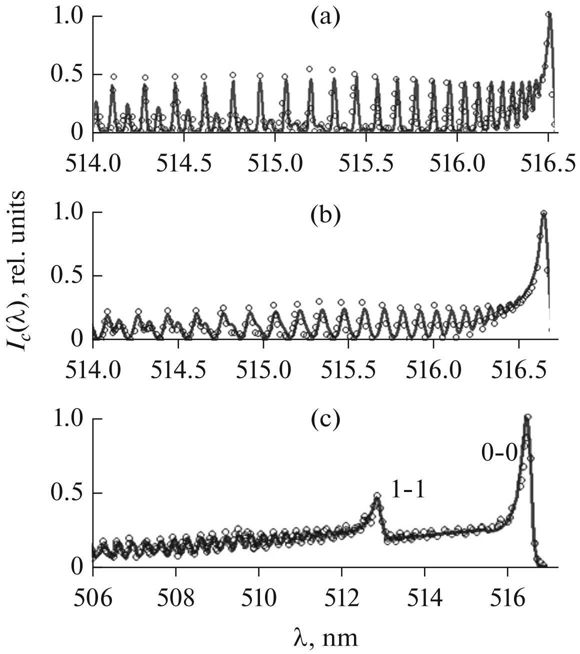

Fig. 14. Radiation intensity $I_c(\lambda)$ in the bands of the Swan system of the C_2 molecule calculated by models from [27–29] (symbols) and this work (curve) for the sequence $\Delta v = 0$: (a and b) T_r ($d^3\Pi_g$) = 6000 [27] and 4000 K [28], respectively; (c) T_r ($d^3\Pi_g$) = 4000 K and T_v ($d^3\Pi_g$) = 5000 K for v = 0–1 [29].

CONFLICT OF INTEREST

The authors declare that they have no conflicts of interest.

REFERENCES

1. Takita, K., Uemoto, T., Sato, T., et al., *J. Propul. Power*, 2000, vol. 16, no. 2, p. 227.
2. Jacobson, L.S., Gallimore, S.D., Schetz, J.A., and O'Brien, W.F., *J. Propul. Power*, 2003, vol. 19, no. 2, p. 170.
3. Klimov, A., Bityirin, V., Brovkin, V., et al., Optimization of plasma generators for plasma assisted combustion, AIAA-2001-2874.
4. Anikin, N., Pancheshnyi, S., Starikovskaia, S., and Starikovskii, A., Air plasma production by high-voltage nanosecond gas discharge, AIAA-2001–3088.
5. Esakov, I.I., Grachev, L.P., Khodataev, K.V., and van Wie, D.M., Investigation of the undercritical microwave streamer discharge for jet engine fuel ignition, AIAA-2001–2939.
6. Chernikov, V., Ershov, A., Shibkov, V., et al., Gas discharges in supersonic flows of air–propane mixtures, AIAA-2001–2948.
7. Leonov, S., Bituirin, V., Savelkin, K., and Yarantsev, D., in *Proc. 4th Workshop on Magnetoplasma*

Aerodynamics for Aerospace Applications, Moscow, 2002, p. 56.

8. Inshakov, S.I., Skvortsov, V.V., Rozhkov, A.F., Shakhatov, V.A., Inshakov, I.S., Uspenskii, A.A., and Urusov, A.Yu., *High Temp.*, 2019, vol. 57, p. 798.
9. Ivanov, V.V., Skvortsov, V.V., Efimov, B.G., Pyndyk, A.M., Kireev, A.Yu., Krasheninnikov, V.N., and Shilenkov, S.V., *High Temp.*, 2008, vol. 46, no. 1, p. 3.
10. Efimov, B.G., Ivanov, V.V., Inshakov, S.I., Skvortsov, V.V., and Starodubtsev, M.A., *High Temp.*, 2011, vol. 49, no. 4, p. 479.
11. Skvortsov, V.V., *Aerodinamicheskie issledovaniya pri uchastii potokov sintezirovannoi i nizkotemperaturnoi plazmy* (Aerodynamic Studies with the Participation of Flows of Synthesized and Low-Temperature Plasma), Moscow: Fizmatlit, 2013.
12. Shakhatov, V.A., *Doctoral (Phys.–Math.) Dissertation*, Moscow: Moscow State Univ., 2016.
13. Ochkin, V.N., *Spektroskopiya nizkotemperaturnoi plazmy* (Spectroscopy of Low-Temperature Plasma), Moscow: Fizmatlit, 2006.
14. Herzberg, G., *Molecular Spectra and Molecular Structure*, vol. 1: *Diatomic Molecules*, New York: Van Nostrand, 1939.
15. El'yashevich, M.A., *Atomnaya i molekulyarnaya spektroskopiya* (Atomic and Molecular Spectroscopy), Moscow: Fizmatlit, 1962.
16. Plastinin, Yu.A., in *Svoistva gazov pri vysokikh temperaturakh* (Properties of Gases at High temperatures), Moscow: Nauka, 1967, p. 82.
17. Kovacs, I., *Rotational Structure in the Spectra of Diatomic Molecules*, Budapest: Akademiai Kiado, 1969.
18. Kuznetsova, L.A., Kuz'menko, N.E., Kuzyakov, Yu.Ya., and Plastinin, Yu.A., *Veroyatnosti opticheskikh perekhodov dvukhatomnykh molekul* (Probabilities of Optical Transitions of Diatomic Molecules), Khokhlov, R.V., Ed., Moscow: Nauka, 1980.
19. Demtreder, V., *Lazernaya spektroskopiya: Osnovnye printsipy i tekhnika eksperimenta* (Laser Spectroscopy: Basic Principles and Experimental Technique), Moscow: Nauka, 1985.
20. *Fiziko-khimicheskie protsessy v gazovoi dinamike. Spravocnik* (Physical and Chemical Processes in Gas Dynamics: Handbook), vol. 1: *Fiziko-khimicheskaya kinetika i termodinamika* (Physico-Chemical Kinetics and Thermodynamics), Chernii, G.G. and Losev, S.A., Eds., Moscow: Nauchno-Izd. Tsentr. Mech., 1982.
21. Pearse, R.W.B. and Gaydon, A.G., *The Identification of Molecular Spectra*, London: Chapman and Hall, 1941.
22. Jeunehomme, M. and Schwenker, R.P., *J. Chem. Phys.*, 1965, vol. 42, p. 2406.
23. Danylewich, L.L. and Nicholls, R.W., *Proc. R. Soc. London, Ser. A*, 1974, vol. 339, p. 197.
24. Cooper, D.M. and Nicholls, R.W., *J. Quant. Spectrosc. Radiat. Transfer*, 1975, vol. 15, p. 139.
25. Curtis, L., Engman, B., and Erman, P., *Phys. Scr.*, 1976, vol. 13, p. 270.
26. Cooper, D.M., Absolute measurements of the electronic transition moments of seven band systems of the C_2 molecule, *PhD Thesis*, Toronto: York Univ., 1979.
27. Coitout, H. and Faure, G., *Spectrosc. Lett.*, 1996, vol. 29, no. 7, p. 1201.
28. Nasser, H., *J. Phys.: Conf. Ser.*, 2014, vol. 511, 012066.
29. Mizeraczyk, J., Hrycak, B., Jasinski, M., and Dors, M., *Int. J. Plasma Environ. Sci. Technol.*, 2012, vol. 6, no. 3, p. 239.
30. Caubet, P. and Dorthe, G., *Chem. Phys. Lett.*, 1994, vol. 218, p. 529.
31. Arnold, J.O., *J. Quant. Spectrosc. Radiat. Transfer*, 1968, vol. 8, p. 1781.
32. Bongers, W., Bouwmeester, H., Wolf, B., Peeters, F., Welzel, S., Bekerom, D., den Harder, N., Goede, A., Graswinckel, M., Groen, P.W., Kopecki, J., Leins, M., van Rooij, G., Schulz, A., Walker, M., and van de Sanden, R., *Plasma Process. Polym.*, 2017, vol. 14, p. 1600126.

Translated by O. Ponomareva